PHYSICAL REVIEW B **92**, 104509 (2015)

Mass superflux in solid helium: The role of ^{3}He impurities

Ye. Vekhov and R. B. Hallock
Laboratory for Low Temperature Physics, Department of Physics, University of Massachusetts, Amherst, Massachusetts 01003, USA
(Received 26 June 2015; published 14 September 2015)

Below ~630 mK, the ^{4}He atom mass flux F, which passes through a cell filled with solid hcp ^{4}He in the pressure range 25.6–26.4 bar, rises with falling temperature and, at a temperature T_d, the flux drops sharply. The flux above T_d has characteristics that are consistent with the presence of a bosonic Luttinger liquid. We study F as a function of ^{3}He concentration, $\chi = 0.17$–220 ppm, to explore the effect of ^{3}He impurities on the mass flux. We find that the strong reduction of the flux is a sharp transition, typically complete within a few mK and a few hundred seconds. Modest concentration-dependent hysteresis is present. We find that T_d is an increasing function of χ and the $T_d(\chi)$ dependence differs somewhat from the predictions for bulk phase separation for T_{ps} vs χ. We conclude that ^{3}He plays an important role in the flux extinction. The dependence of F on the solid helium density is also studied. We find that F is sample dependent, but that the temperature dependence of F above T_d is universal; data for all samples scale and collapse to a universal temperature dependence, independent of ^{3}He concentration or sample history. The universal behavior extrapolates to zero flux in the general vicinity of $T_h \approx 630$ mK. With increases in temperature, it is possible that a thermally activated process contributes to the degradation of the flux. The possibility of the role of disorder and the resulting phase slips as quantum defects on one-dimensional conducting pathways is discussed.

DOI: 10.1103/PhysRevB.92.104509 PACS number(s): 67.80.bd, 71.10.Pm

I. INTRODUCTION

Solid helium is a unique substance that displays a combination of classical and quantum properties. It has been extensively studied both experimentally and theoretically for many decades. One of the most interesting properties of *liquid* helium is superfluidity, a state of matter in three dimensions than occurs below a pressure-dependent temperature T_λ. This quantum property is strongly affected by spatial limitation. In the two-dimensional (2D) case, the phase transition from the superfluid phase to the normal phase is related to the unbinding of vortices, as described by Berezinskii *et al.* [1,2]. In one dimension (1D), another sort of quantum point defect, the so-called phase slip, is responsible for this transition. Quantum Monte Carlo (QMC) simulation [3] predicted that the cores of screw dislocations in solid helium should be an example of 1D superfluidity. The flow of superfluid helium in 1D can be described by the quantum hydrodynamic theory known as Luttinger liquid theory [4]. This idea has been confirmed by large-scale QMC simulations [5–7] for the case of nanopores. The basic requirements for 1D channels to demonstrate Luttinger liquid behavior [8] are that the pore diameter is sufficiently small, the pore length is sufficiently long, and the temperature is low enough with respect to T_λ.

We developed an apparatus, the so-called UMass Sandwich [9], to study the possible ability of solid helium to carry a helium mass flux [10–12]. Using porous media (here, Vycor rods), we are able to apply a chemical-potential difference between two separated regions in a solid ^{4}He sample without mechanically squeezing the solid helium lattice itself. It was found that an experimental cell filled with solid ^{4}He can carry a flux [10], but only below some characteristic temperature T_h, and the flux rate substantially increases with decreasing temperature. It can be reduced and eliminated with an increase in pressure [11]. Tiny amounts of the impurity ^{3}He also change the flux dramatically [13] at a characteristic low temperature T_d. A brief report that discusses some of the ^{3}He concentration dependence has appeared [13]. Here, we will describe our measurements as a function of the ^{3}He concentration at several pressures in more detail and discuss our interpretations of the role of the ^{3}He. We will also offer comments on several flow scenarios, including one-dimensional pathways.

We note here that this report corrects a thermometry error that caused a small shift in the temperature scale below ~100 mK that was used in the work reported previously in Ref. [13]. This was caused by a change in the room-temperature electronics which we subsequently determined introduced a small but measurable heating of the thermometer used to measure the solid helium temperature. The temperature correction [14] for the work reported in Ref. [13] is less than 1 mk above 120 mK, 5.5 mK at 80 mK, and can be found from $TC_{\mathrm{new}} = TC - 0.09637 \exp(-TC/0.02755)$. TC is the temperature of the thermometer affixed to the experimental cell (Fig. 1) and is used to define the solid helium temperature T. All temperatures reported in this work include this correction.

II. EXPERIMENTAL TECHNIQUE

In this work, many freshly grown (and some partially annealed) solid ^{3}He-^{4}He mixture samples have been used to study the effect of the ^{3}He impurity concentration χ (in the range $0.17 < \chi < 220$ ppm), temperature, and pressure on the ^{4}He mass flux. Our experimental methods have been described in substantial detail in Refs. [10–12]. We provide a brief discussion of our approach here.

A. Sample preparation

Solid helium samples are grown at constant temperature from the superfluid in the temperature range $0.3 < T < 0.4$ K by the condensation of helium into a sample cell (volume, $V = 1.84$ cm^3) through a direct-access heat-sunk capillary (capillary 3 in Fig. 1) followed by an increase in the pressure up to near the melting pressure (about 25.34 bar). Subsequent

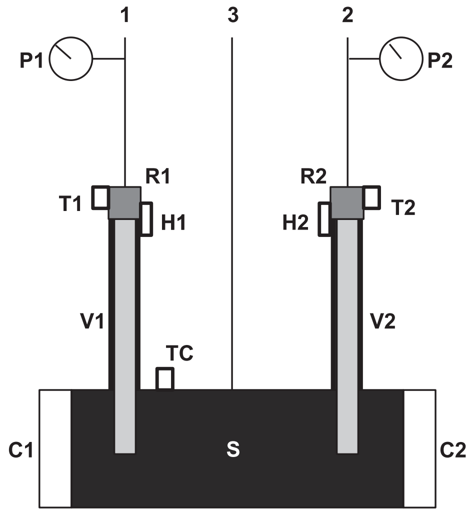

FIG. 1. Schematic diagram of the cell used for flow experiments. Two capillaries, 1 and 2, go to liquid reservoirs $R1$ and $R2$ at the top ends of the Vycor rods, $V1$ and $V2$. Capillary 3 enters from the side of the cell and is used for adding helium to the cell. Two capacitance pressure gauges, $C1$ and $C2$, are located on either end of the cell for *in situ* pressure measurements of the solid ^{4}He. Pressures in the lines 1 and 2 are read by pressure gauges, $P1$ and $P2$, outside the cryostat. Each reservoir has a heater, $H1$ and $H2$, which prevents the liquid in it from freezing and allows the temperatures of the reservoirs to be controlled. The relevant temperatures are read by calibrated carbon resistance thermometers $T1$, $T2$, and TC. (Reproduced from Fig. 1 in Ref. [11].)

additions of helium are by means of two other capillaries (1,2 in Fig. 1) in series with Vycor (porous glass with interconnected pores of diameter ≈7 nm) rods (0.14 cm diameter, 7.62 cm length). Helium is added to the Vycor to inject atoms and create the solid at the desired pressure in the range of $25.6 < P < 26.4$ bar. A cold plate at the base of the sample cell is thermally connected to the mixing chamber of the dilution refrigerator and, when the cell is filled with solid ^{4}He, it can be cooled to about 60 mK. The lowest temperature of the cell is limited by the characteristics of our 1970s vintage refrigerator and the heat flux through the superfluid-filled Vycor rods. Their warmer ends have to have much higher temperature than the temperature of the solid-filled cell, up to 1.5 K, to prevent the formation of solid helium in the two reservoirs, $R1$ and $R2$, and at the interface between the Vycor rods and the reservoirs. The pressure and temperature ranges available have upper limits due to the need to maintain an adequate value of the superfluid density in the reservoir and the Vycor so as to not restrict the flux of helium in places external to the solid-filled cell.

To create samples of known ^{3}He concentration, the cell is emptied between each set of measurements [13]. The cell is then filled with nominally pure ^{4}He liquid (0.17 ppm ^{3}He) up to the saturated vapor pressure through use of line 3. Then, a small calibrated volume at room temperature is filled with pure ^{3}He to a known pressure. This is injected into the cell via line 3 and this injection is followed by additional ^{4}He, which also enters through line 3, to bring the cell close to the melting curve. With knowledge of the relevant volumes and pressures, a known concentration of ^{3}He is thus introduced into the cell.

The solid is then grown by injection of ^{4}He through the two Vycor rods. After the sample is grown, it is allowed to rest for ≈5–10 hours at a solid helium temperature ⩽0.4 K before starting any measurements. Most solid helium samples are freshly grown (and not annealed above 0.5 K). As we will see, we find reproducibility in a given sample with temperature changes, which suggests that the samples are adequately in equilibrium after being created. As we reported previously for nominal-purity well helium (measured for this work to be ∼0.17 ppm ^{3}He concentration), high-temperature annealing leads, on cooling, either to a substantial flux decrease or to complete flux extinction, with in that case no evidence for flux at lower temperatures.

B. Measurement procedure

To initiate the flux, an initial chemical potential difference $\Delta\mu_0$ is applied between the tops of the Vycor rods by changing the temperatures, $T1$ and $T2$, of the two reservoirs, $R1$ and $R2$, to create a temperature difference between them (see Fig. 1). This creates a flux due to the fountain effect, which is seen by observing changes in $P1$ and $P2$. Since we monitor the pressures and the temperatures as a function of time, the chemical potential $\Delta\mu$ can be calculated,

$$\Delta\mu = \int \frac{dP}{\rho} - \int S dT, \tag{1}$$

where ρ and S are the temperature-dependent density and entropy of liquid helium, respectively. In contrast to some of the earlier work from our laboratory [11], where $\Delta P = P1 - P2$ was applied by direct mass injection, our current study uses the application of a temperature difference [15] $\Delta T = T1 - T2$. This approach offers two advantages. It allows for smaller density changes in the solid helium than was the case for direct injection of ^{4}He to the sample cell through one of the lines, 1 or 2. And it allows us to keep constant the total amount of ^{4}He in the apparatus.

An example of the procedure used for the flux measurements for a solid ^{4}He sample with a 10.2 ppm ^{3}He impurity content is shown in Fig. 2. The creation of a change in the energy deposited in heaters $H1$ and $H2$ results in a temperature difference, $\Delta T = T1 - T2$, between the reservoirs [Fig. 2(a)], $R1$ and $R2$, at the tops of the Vycor rods. This results in pressure responses [Fig. 2(b)], $P1$, $P2$, and $\Delta P = P1 - P2$ due to the fountain effect at a sequence of rising solid helium temperatures [Fig. 2(c)], TC. The derivative of ΔP,

$$F = \frac{d(P1 - P2)}{dt}, \tag{2}$$

is taken to be reasonably proportional to the flux F of atoms that move from one reservoir to the other. We report the rate of pressure change in mbar/s units, where 0.1 mbar/s corresponds to a flux of $\approx 4.8 \times 10^{-8}$ g/s.

We use measurements of F of this sort in two related ways. In one, we study how the flux F depends on the chemical potential $\Delta\mu$ as time evolves. The chemical potential changes from its initially imposed peak value $\Delta\mu_0$, imposed by the initial ΔT, to zero as equilibrium is restored by the creation of a fountain-effect-induced pressure difference, $P1 - P2$. In the other, we study, for a given value of the imposed ΔT, how

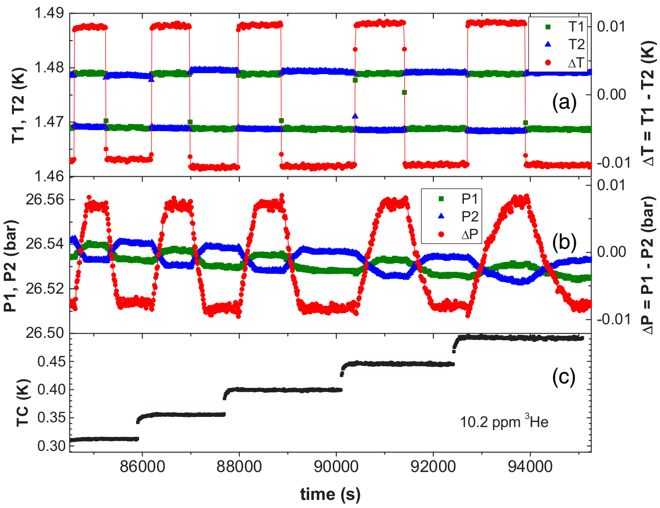

FIG. 2. (Color online) An example of flux measurements for a 10.2 ppm sample. (a) Here, temperatures are established for each of the reservoirs, held constant while the pressure in each of the reservoirs stabilizes, and then the temperature values of the two reservoirs are interchanged. The interchange results in a flux of atoms driven by the fountain effect, which is recorded by (b) the pressure gauges $P1$ and $P2$. The rate of change of $P1 - P2$ provides a measure of the time-dependent flux. (c) The solid ^{4}He temperature is changed and the process continues for a sequence of solid ^{4}He temperatures, TC.

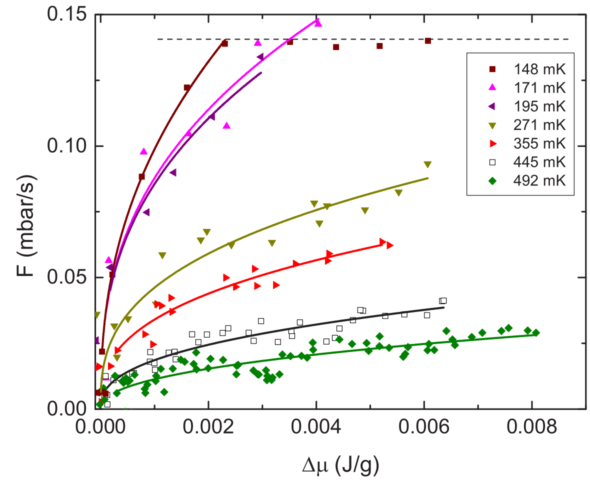

FIG. 3. (Color online) An example of the $F(\Delta\mu)$ dependence for different solid helium temperatures for the case of a sample with a ^{3}He concentration of 10.2 ppm. Solid lines are power-law fits by use of Eq. (3). The dashed line is the upper limit of the flux due to the Vycor bottleneck for reservoir temperatures of 1.48 K (see Fig. 3 in Ref. [16]). Note that before taking a derivative to calculate F, a moving average of the $\Delta P(t)$ data (see Fig. 2) was determined: by 3 points for $TC < 0.25$ K, by 7 points for $0.25 < TC < 0.40$ K, by 9 points for $TC = 0.445$ K, and by 12 points for $TC = 0.492$ K.

the maximum resulting flux F depends on the temperature of the solid ^{4}He. Data, of the sort shown in Fig. 2 for a specific 10.2 ppm ^{3}He sample, is taken for a variety of solid helium samples, each with a specific value of the ^{3}He concentration. We choose to focus on the behavior of ΔP, which also allows us to eliminate a small long-term drift in $P1$ and $P2$, which is typically present in our long-duration measurements due to main helium bath level changes. Our basic conclusions are not changed if instead we focus on the individual behaviors of $P1$ or $P2$.

C. Flux dependence on $\Delta\mu$

Using data, including that in Fig. 2, F vs $\Delta\mu$ is obtained for positive ΔT values and presented in Fig. 3 for a set of solid helium temperatures. The maximum flux values are typically constrained by the solid helium sample. But for the lower cell temperatures, the constraint can be imposed by the temperature of the reservoir at the upper end of the Vycor which restricts the magnitude of the flux, as shown previously [16]. The dashed line in Fig. 3 represents the flux limit imposed by the Vycor. Similar behavior is seen for negative ΔT values. As was found earlier [12], a power law provides a good two-parameter characterization for data of this sort,

$$F = A(\Delta\mu)^b, \tag{3}$$

where A and b are fit parameters. Within our errors, the parameter b is independent of temperature, but depends on pressure. In the pressure range of our study, b is less than 0.5 [12]. We will return to a discussion of the characteristics of A and b later.

D. Flux dependence on temperature

The maximum flux measured through the solid helium that results from a specific imposed ΔT (typically ± 10 mK in Fig. 2) occurs for a resulting $\Delta\mu$ in the range 5–8 mJ/g, and has a temperature dependence as illustrated in Fig. 4. This is for the case of a different solid sample with a ^{3}He concentration of 19.5 ppm. As we will see, this temperature dependence is present for all of the concentrations we have studied. This maximum flux F increases with falling temperature, with warming and cooling showing the same values of the flux for a given sample, as long as the sample is not annealed. And

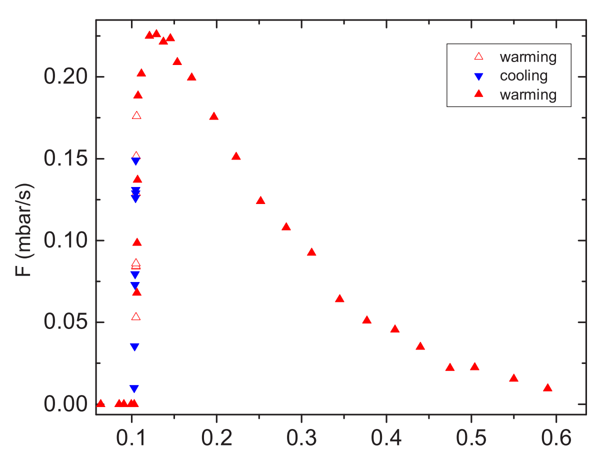

FIG. 4. (Color online) Maximum values for the flux as a function of temperature for the case of a solid with 19.5 ppm ^{3}He at $P = 26.40$ bar. The sharp behavior of the flux extinction in a very narrow range of temperature near $T = T_d$ is evident.

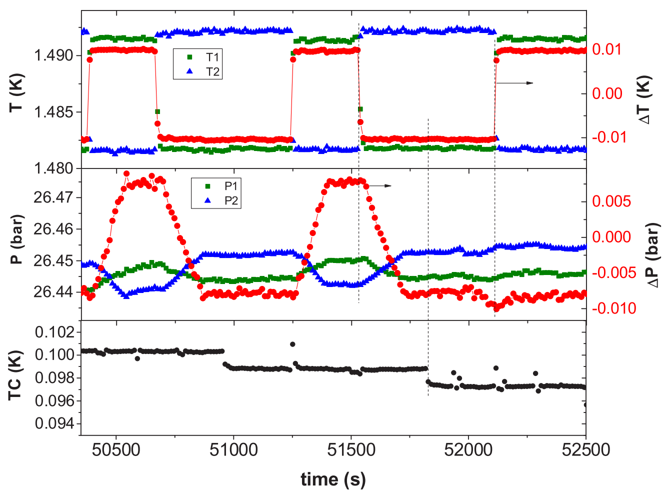

FIG. 5. (Color online) An example of the extinction of the flux as the temperature of the solid helium falls below $T = T_d$ for a 10.2 ppm ^{3}He sample at $P = 26.30$ bar. This figure has the corrected temperature scale and is a revision of the similar figure presented in Ref. [13].

there is a sharp, hysteretic, reversible decrease of the flux at a concentration-dependent temperature T_d.

As seen in Fig. 4 for this $\chi = 19.5$ ppm ^{3}He impurity sample, the flux that results from a given ΔT is an increasing function of decreasing temperature until the temperature drops below $\sim$105 mK, below which there is no flux. As an illustration of just how sharp and prompt the extinction behavior is, consider Figs. 5 and 6. These figures illustrate that for a $\chi = 10.2$ ppm sample, the transition from flux to no flux is no more than $\approx$1.5 mK wide, with the cessation of the flux complete within no more than $\sim$350 seconds. Similarly, in Fig. 6, we see that there is no flow at a cell temperature of 99 mK, but that an increase in the cell temperature to a

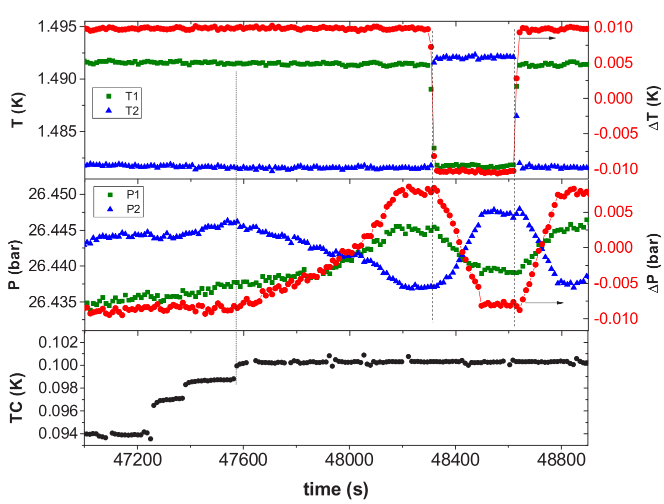

FIG. 6. (Color online) An example of the recovery of the flux near $T = T_d$ for the same 10.2 ppm sample as in Fig. 5. No flux is seen in the presence of an imposed ΔT until the cell temperature increases above about 100 mK, after which the flux recovers in a few hundred seconds. This figure has the corrected temperature scale and is a revision of the similar figure presented in Ref. [13].

TABLE I. Sample characteristics. The ^{3}He concentration (ppm) is in two cases estimated (*) based on the $ln(\chi)$ vs $1/T$ linear dependence shown in the inset of Fig. 13. The quantities $\delta\chi$ and δT_d represent uncertainties in the determination of χ and T_d.

χ	$\delta\chi$	P (bar)	T_d (mK)	δT_d (mK)
0.17		25.64	72.5	7
0.17		25.90	72.5	3
1.0	0.2	25.86	80.5	5
2.0	0.2	26.10	88.5	5
4.0	0.5	26.09	91.5	5
10.2	0.5	26.30	97.0	5
15.0	3	25.92	99.5	3
19.5	1	26.40	103	3
25.5	1.2	26.12	106	3
40.0*	5	26.15	109	2
61.0	3	26.36	111	2
119.3	6	26.40	115.5	2
220.0*	30	25.90	125	2

fixed value near 100 mK results in a growth of the flux, with a flux recovery time of $\sim$600 seconds. The difference in the temperature of the sharp change in F between cooling and warming shows a small hysteresis at this value of the ^{3}He concentration. The sharp gradient in the slope of F vs T near 100 mK seen in Fig. 4 is stable. That is, if the temperature remains fixed, then the value of F remains stable at any point in the T_d transition region [17].

Now, the time noted for the flux to make the no-flow to flow recovery (or the reverse) likely places some constraints on scenarios for what causes the transition from a state of no flow to a state of flow. One possibility is that it takes this long for the temperature of the solid to change. To explore this, a calculation for our cylindrical geometry that incorporates the Kapitza resistance between the solid and the copper wall and the properties of solid helium has been done by Mullin [18], with the result that the time for this thermal equilibration to take place is predicted to be no more than $\sim$50 msec. This result is geometry dependent, but generally consistent with the thermal equilibration experiments carried out by Huber and Maris [19]. That work indicated that equilibration near 100 mK is achieved in $\sim$10 msec. These facts indicate that the equilibration time for temperature of the solid is much faster than the observed recovery times and thus the flux change must be related to the movement of the ^{3}He and not due to a thermal time constant. We will discuss this further below.

E. Flux dependence on ^{3}He concentration

The same procedure shown in Fig. 2 has been used for a substantial set of solid helium samples with different ^{3}He impurity concentrations χ, which ranged from a low for nominal well helium of 0.17 ppm ^{3}He to a high of 220 ppm, as listed in Table I. Two examples of the mass flux temperature dependencies are shown in Figs. 7 and 8 for $\chi = 0.17$ and 2 ppm, respectively. Data points here represent the maximum flux values normalized to the maximum flux rate at 200 mK to facilitate the comparison. The relevance of such normalization will become more apparent shortly.

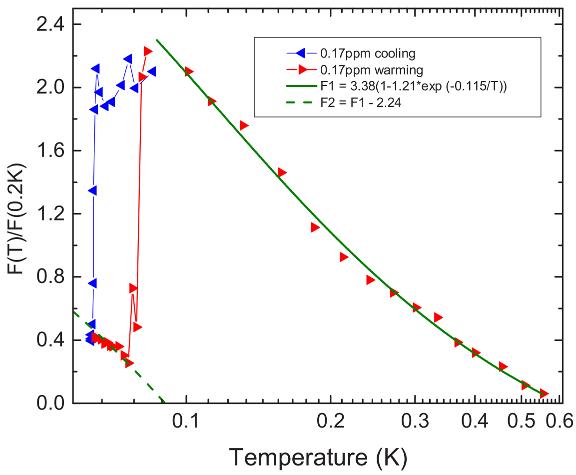

FIG. 7. (Color online) An example of flux reduction and hysteresis near $T = T_d$ for a 0.17 ppm ^{3}He and $P = 25.64$ bar sample. The smooth curve will be discussed in the next section.

Figures 7 and 8 document hysteresis in the vicinity of T_d with the flux drop during cooling typically taking place at slightly lower temperature than the flux rise during warming. This hysteresis is measurable at most of the ^{3}He concentrations studied and may be considered as a feature of a first-order phase transition. This suggests that phase separation may be important and we will return to this point later. The hysteresis is most evident at the lowest concentrations. The width of this hysteresis for low concentrations is shown in Fig. 9. Figures 7 and 8 demonstrate that for low concentrations, the flux does not drop to zero and recovers on cooling below $T < T_d$. The recovery of the flux as the temperature is lowered below T_d [13,20] suggests that the role played by the ^{3}He saturates. We will return to this point in Sec. IV. The dashed curves on the figures are vertically shifted continuations of the solid smooth curves, which serve to characterize the data. The significance of these smooth curves will be discussed in the next section. If χ is more than about 10 ppm, e.g., as shown in Fig. 4,

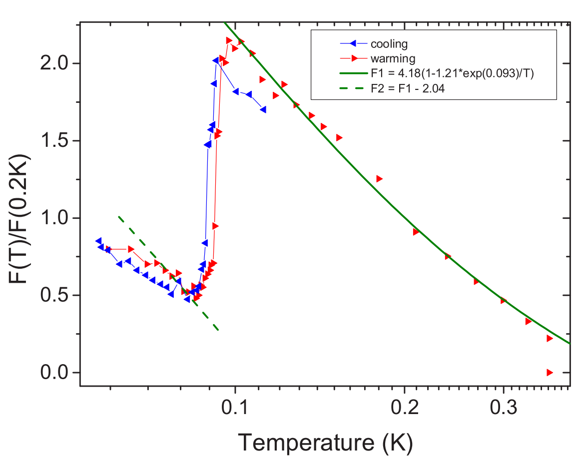

FIG. 8. (Color online) An example of flux reduction and hysteresis near $T = T_d$ for a 2.0 ppm ^{3}He and $P = 26.10$ bar sample. The smooth curve will be discussed in the next section.

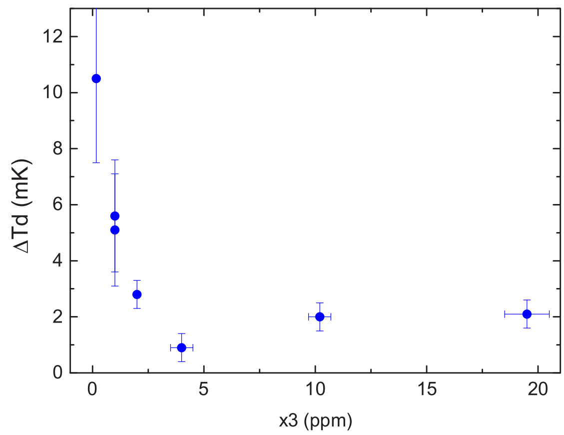

FIG. 9. (Color online) The width of the hysteresis seen in the vicinity of $T = T_d$ for low ^{3}He concentrations. The width of the hysteresis region narrows steeply with increasing concentration.

then there is no flux recovery down to $\sim$60 mK (the lowest temperature for these measurements).

Data for a range of samples with different concentrations and sample histories are shown in Fig. 10. In each case, the maximum flux value shown is that which results from the same value of the imposed ΔT. The shift in T_d with concentration is evident. Different samples with different histories at a given concentration have somewhat different absolute values of F, but the temperature dependence and value of T_d are reproducible for a given concentration.

III. DISCUSSION

A. Universal temperature dependence

We now present in more detail the temperature dependence for temperatures above T_d. As we will show, the temperature

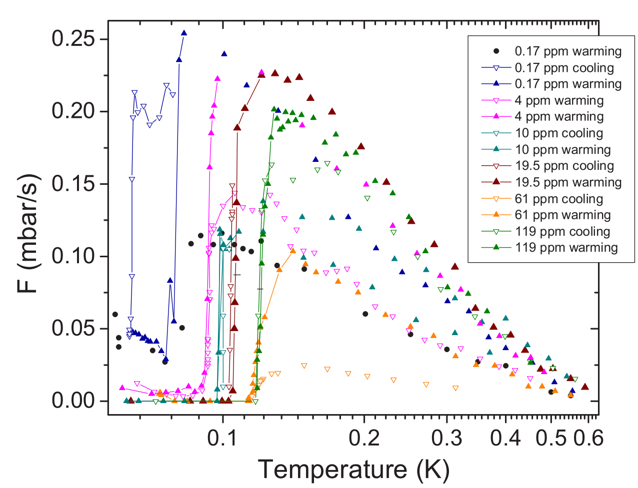

FIG. 10. (Color online) The temperature dependence of the flux observed for ^{4}He with several ^{3}He impurity concentrations and experimental conditions, determined in each case with a constant value of ΔT, which yields a maximum flux F that appears for $\Delta\mu$ in the range 5–8 mJ/g. This figure has the corrected temperature scale and is a revision of the similar Fig. 1 presented in Ref. [13]. For each data set, the solid pressure was in the range 26 ± 0.4 bar.

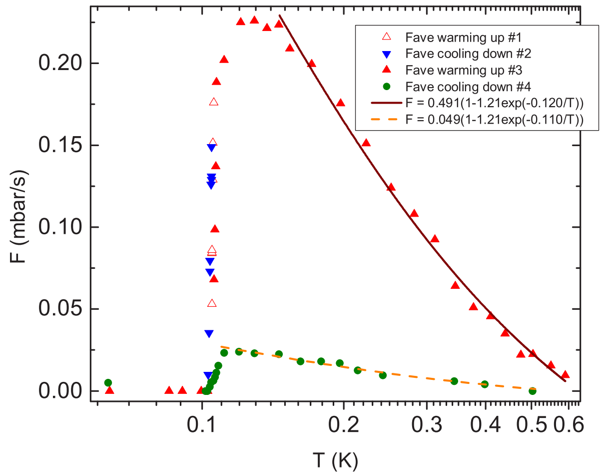

FIG. 11. (Color online) An example of flux extinction near $T = T_d$ for a 19.5 ppm ^{3}He sample at $P = 26.40$ bar sample. For comparison, data for cooling is shown (solid circles) after the flux ceased at $T = 0.625$ K. Note that the flux values are shown in mbar/s units.

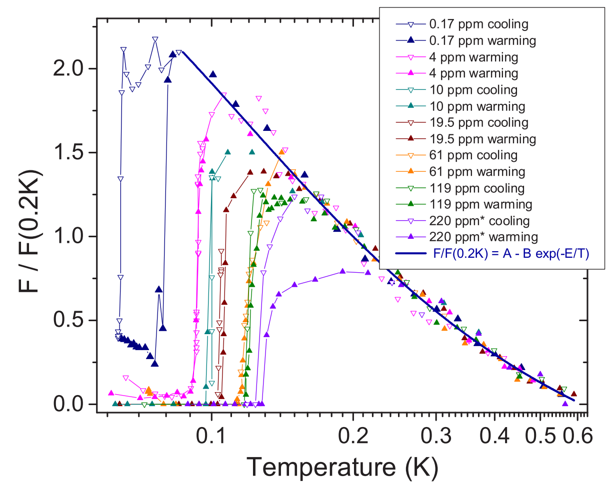

FIG. 12. (Color online) The temperature dependence of the normalized flux observed for ^{4}He with several ^{3}He impurity concentrations and experimental conditions, with the solid ^{4}He pressure 26 ± 0.2 bar. Fitted line: see text.

dependence for $T > T_d$ is robust, but the absolute value of the flux depends importantly on the sample and its history. As an example of the sort of variability that we have found, consider the data shown in Fig. 11 for the sample with $\chi = 19.5$ ppm. The flux values are presented here in mbar/s units (not normalized values) in order to compare the behavior of the flux before and after the temperature was increased to 620 mK, where the flux was no longer measurable. When cooled, after the sample cell was warmed, the flux was greatly reduced (circles). The data set for the larger values of F shown here is the same data set shown in Fig. 4.

What is not immediately apparent in Figs. 10 and 11 is that the temperature dependence at temperatures above the peak flux reached is robust. To demonstrate this most clearly, we normalize the many data sets shown in Fig. 10. We accomplish this by use of a multiplicative factor for each data set to force the various values of F to superimpose at $T = 0.2$ K. The normalized flux temperature dependencies for the samples of different ^{3}He concentrations are presented in Fig. 12.

One can see again here, as was evident in Fig. 10, that the T_d values shift to higher temperatures with higher χ values. At the same time, $F(T)$ for different samples at $T > T_d$ collapse to a universal temperature dependence [13]. This figure also shows that in the temperature range in the vicinity of the peak value of the flux (near $T = T_d$), the peak becomes more rounded with less curvature for larger χ values.

T_d values determined from the data in Fig. 12 and other data like them are shown in Fig. 13 to show how the ^{3}He concentration affects T_d. Because there is hysteresis, we define T_d to be the average of the value of the temperature at the foot of the cooling and warming data sets. It is natural to compare these temperature-dependent data to the data on phase separation in solid helium. According to Ref. [21], extrapolated to 26 bar, the temperature of solid-solid (bcc ^{3}He-rich inclusions form inside the hcp ^{4}He-rich matrix) phase-separation temperature T_{ps} can be found from

$$T_{ps} = [0.80(1 - 2\chi) + 0.14]/\ln(1/\chi - 1), \qquad (4)$$

and this is represented in Fig. 13 by the dashed line. The number 0.80 in this expression comes from the extrapolation to the pressure of our experiment. In the case of bulk phase separation for our pressure range, another situation is present: liquid ^{3}He-rich regions form inside the solid ^{4}He matrix (the so-called solid-liquid case). This scenario was calculated in Ref. [13] and is shown by the solid line in the same figure. It can be seen here that our T_d vs χ dependence has a shape similar to, but lies above, the solid-liquid case for phase separation. This will be discussed further in Sec. III C.

In an attempt to further characterize the data, we have utilized several functions. In recent presentations [12,13], we have favored $F = A - B\exp(-E/T)$, which is motivated by the thought that some thermally activated process may be relevant. Independent fits of this functional dependence to all of the data sets results in the characterization of the universal behavior of the temperature dependence. We find a

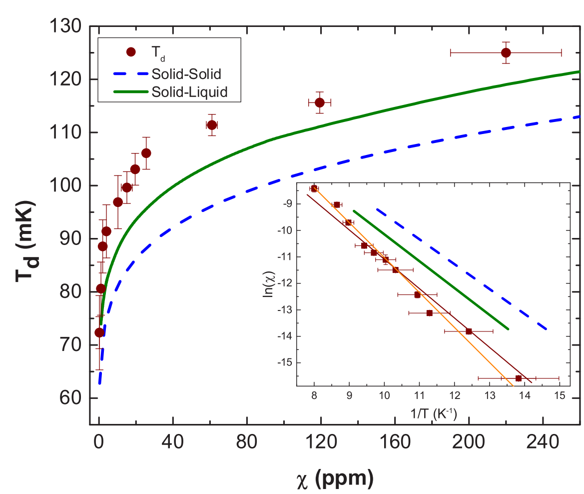

FIG. 13. (Color online) Temperature of the sharp drop in F, T_d. Inset: $ln(\chi)$ vs $1/T$; see text. This figure has the corrected temperature scale and is a revision of the similar Fig. 5 presented in Ref. [13].

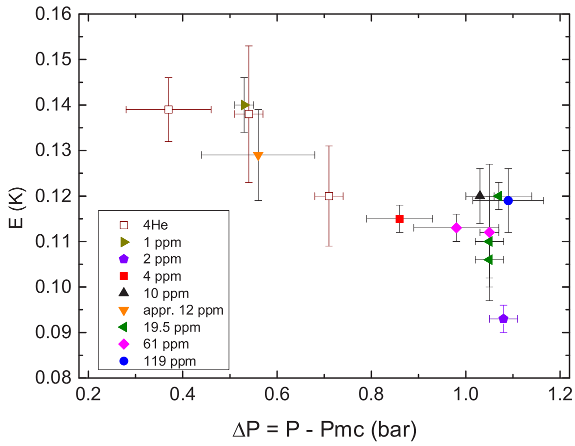

FIG. 14. (Color online) Pressure dependence of the parameter E.

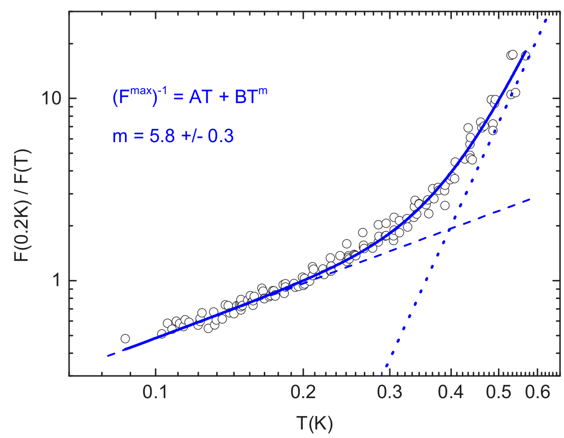

FIG. 15. (Color online) Temperature dependence of the flux resistance, $(F)^{-1}$, measured through the solid sample (see Ref. [13], Fig. 4) and presented here on a log-log scale. The solid line is a fit of the data by Eq. (6) and the dashed and dotted lines represent linear and $T^{5.8}$ behavior, respectively.

good characterization of the data with

$$F = F_0[1 - 1.21 \exp(-E/T)]. \tag{5}$$

The value of E that results from such a characterization of the data depends weakly on pressure, as shown in Fig. 14. The higher the pressure (density), the lower the value of E, i.e., the $F(T)$ dependence gets steeper with pressure. The use of colors for symbols in this figure is the same as in Figs. 11 and 12. There is no apparent dependence of E on χ.

The value of F_0 may be interpreted to be proportional to the number of conducting pathways inside the solid helium, i.e., at $T \sim T_h$, conducting pathways are being partially annealed (completely in some cases) leading to a substantial flux decrease in the whole $T_d < T < T_h$ temperature range on subsequent cooling.

As we have pointed out earlier [16] (e.g., Fig. 9 in that earlier work and the associated comments [16]), the entire temperature dependence is not fully explained by thermal activation since the flux extrapolates to zero at a finite temperature. So, the explanation for whatever controls the decrease in flux with increasing temperature must go beyond simple thermal activation.

As an alternate approach to characterize the temperature dependence, the normalized universal data for $T > T_d$ from Fig. 12 can be inverted, $(F)^{-1}$, to obtain something we might call a flux resistance [22], as shown in Fig. 15. This approach allows us to explore whether there might be any power-law behavior, although the temperature range is very narrow for such an approach. One can see in Fig. 15 that there appears to be a crossover in the behavior of the temperature dependence. The data for the range of samples studied can be described reasonably well by

$$(F)^{-1} = F(0.2K)/F = AT^k + BT^m, \tag{6}$$

where A, B, k, and m are parameters. We find that with the choice of $k = 1$, a fit to the data yields $m = 5.8 \pm 0.3$.

It is an open question as to what the origin is of those two apparently distinct contributions to the temperature dependence of the mass flux resistance. But, such behavior is not without precedent for a quasi-one-dimensional system. Consider, for example, the case of superconducting nanowires below the transition temperature T_c. These nanowires demonstrate nonzero resistance at any finite temperature, apparently due to the presence of phase slips in the order parameter that result in dissipation, which destroys superconductivity. These phase slips are due to thermal fluctuations at higher temperatures close to but below T_c, or to quantum-mechanical tunneling at low temperatures, the so-called quantum phase slips (QPS). Electrical-transport measurements in single-crystal Sn nanowires [23] and its analysis [24] showed a power-law dependence $\rho(T) \sim T^\alpha$ at $T < T_c$ with an exponent $\alpha \approx 5$ for nanowires of diameter 20 and 40 nm, but much larger values of α for larger wire diameters. These data were interpreted in terms of the unbinding of quantum phase slips with temperature. Also it was predicted [25] that in the limit of very thin wires and low temperatures, where unbound QPS behave as a gas, the temperature dependence of the wire resistivity should become linear at the transition to the disordered (i.e., nonsuperconducting) phase. As shown in Fig. 15, the data is consistent with a linear dependence of the flux resistance for the flux that we observe at low temperature. The relationship that might exist between these rather different physical systems, i.e., conducting pathways in solid helium and very thin wires, has not been explored theoretically, but both systems may be describable by Luttinger liquid theory.

B. Luttinger liquid

An example of the nonlinear behavior of F vs $\Delta\mu$ shown in Fig. 3 is reasonably well represented by Eq. (3), where b is less than 0.5, and within our errors is independent of T. An example of the independence of b from temperature is shown in Fig. 16 for $\chi = 10.2$ ppm. Here, as in our earlier measurements for nominal-purity well helium [12], all of the temperature dependence is contained in the amplitude A. We have previously shown that for well helium, b depends on pressure. As we have suggested, this nonlinear behavior and independence of b from temperature supports the possibility that the flux is carried by one-dimensional paths, e.g., perhaps the cores of edge dislocations [12], and can be described by the properties of a so-called bosonic Luttinger liquid [4].

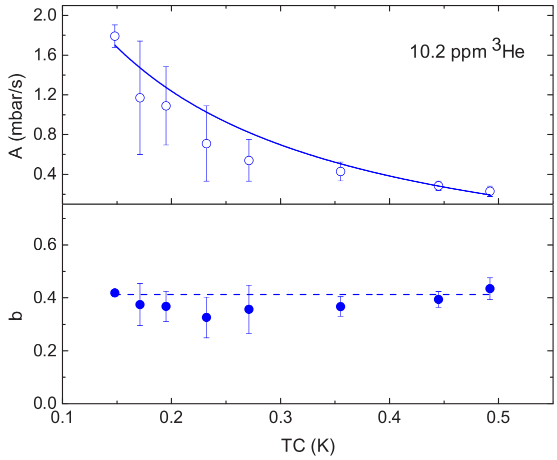

FIG. 16. (Color online) Temperature dependence of fit parameters (a) A and (b) b for the data in Fig. 3; see Eq. (3).

As noted, the exponent b is temperature independent, but it depends on the solid helium pressure. The higher the pressure, the larger is the value of b. Data for b as a function of the distance from the melting curve, $\delta P = P - P_{MC}$, is presented in Fig. 17 for nominally pure (170 ppb) helium as well as for a number of concentrations. Although the number of concentrations for which we have data adequate to determine b for a range of pressures is limited, there is apparently no significant dependence of b on χ.

The data for b above can be used to obtain the pressure dependence of the Luttinger parameter, g. The parameter g provides a measure of the strength of the interactions among the ^{4}He atoms in one dimension. If we presume that we have a number of independent random scattering sites that introduce phase slips, then the Luttinger parameter g can be obtained from b by means of $g = [(1/b) + 1]/2$ [26]. The results shown in Fig. 18 suggest that for such a scenario, we are well in the Luttinger regime, but that with increasing pressure, g decreases and we approach the nonsuperfluid regime. This is consistent

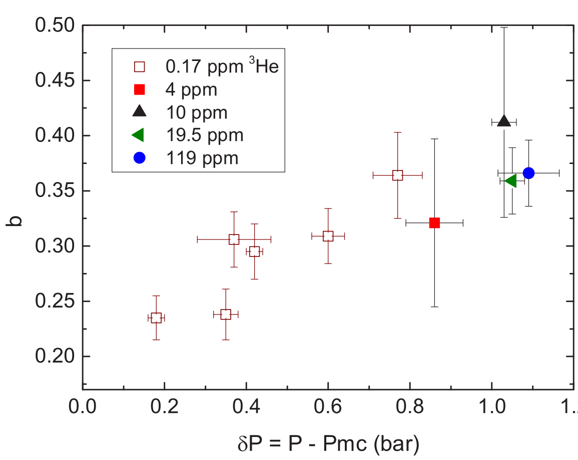

FIG. 17. (Color online) Pressure dependence of the fit parameter b. Open square data points here correspond to nominally pure ^{4}He samples (0.17 ppm ^{3}He) and other data points represent the data for ^{3}He-^{4}He mixtures with $\chi > 0.17$ ppm. Here, δP is the distance above the melting curve in bar.

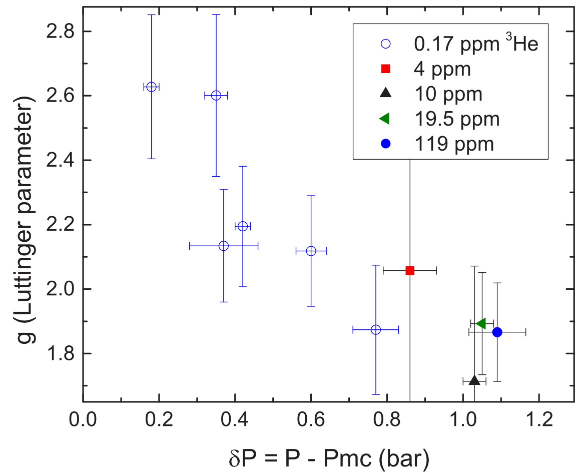

FIG. 18. (Color online) Pressure dependence of the Luttinger parameter g, presuming that $g = [(1/b) + 1]/2$. Again, here, δP is the distance above the melting curve in bar.

with previous work [10,11] in which the flux disappeared at higher pressures. The colors of symbols in Fig. 18 have the same sense as in Fig. 17.

Based on the pressure (density) dependence of g and E, shown in Figs. 18 and 14, respectively, one can see that ^{3}He impurities in the range studied do not affect these data. This suggests that for $T > T_d$, there is no measurable ^{3}He role in either the $F(\Delta\mu)$ or the $F(T)$ dependencies.

C. Comments

We have discussed the effect of ^{3}He impurities on the flux measured and here we summarize the ^{3}He effects that we have observed. First of all, there is a sharp flux extinction at a characteristic temperature T_d, which itself depends on ^{3}He concentration, χ, and this $T_d(\chi)$ dependence (see Fig. 13) is reminiscent of the bulk phase separation shifted to higher temperatures. Another point is that this extinction is a slow process compared with the thermal equilibration time for the solid (∼10's of msec), but a fast process (∼100's of seconds) compared to the time required for complete solid phase separation (dozens of hours [27]) in samples of higher concentrations than we have used here.

These facts suggest that the behavior of the ^{3}He is relevant. It is likely that only a small fraction of ^{3}He is responsible for the flux extinction and this phenomenon is due to ^{3}He redistribution in the vicinity of the phase-separation temperature. Work by Edwards *et al.* [28] indicates deviations from T^3 behavior in the specific heat for mixture solids for $T > T_{ps}$. This suggests local ^{3}He concentration fluctuations [29] are likely relevant to our observations; the ^{3}He fluctuates in position and is thereby able to block the flux at a temperature above the bulk phase-separation temperature. It is the case that for the very low concentrations we have for the most part used in this work, diffusion can be quite fast. This is true whether the ^{3}He considered is in the solid mixture or elsewhere in a liquid mixture. We will explore this further below.

Based on the $F \sim (\Delta\mu)^b$ dependence, as was already shown in Ref. [12], we suggested that the flux could be consistent with a one-dimensional scenario. One can envision candidates for these 1D pathways: (1) liquid channels, e.g., between grain boundaries and the sample cell wall [30], or (2) the cores of dislocations in solid helium. But a number of other possibilities come to mind and have at times been discussed. In an effort to be reasonably complete, we will discuss them, at least briefly, here. In doing so, we will offer comments and also present some qualitative numerical calculations that relate to the ^{3}He.

It has at times been suggested that the mass flux seen to exist between the two reservoirs might not be an actual flux through the solid, but instead a crystallization of the solid where mass enters and a melting where mass leaves. We believe that this is not likely. Substantial evidence that this is not the explanation is found in the behavior of the flux when the history of the sample includes an increase in temperature above 650 mK and a subsequent cool down to low temperatures. When this sort of protocol is followed, it is typically the case that the warming-cooling cycle results in a substantial reduction of the flux or its elimination. We believe that were the suggested crystallization process at work, it should not be much modified by such a cycle. Instead, we believe that such a cycle, i.e., an annealing cycle, modifies the flow paths that exist.

1. *Liquid channels*

Although we have previously argued that liquid channels are likely not responsible for the flux, we discuss them further here. Were they present, the superfluid density in them could be reduced or eliminated by the migration of ^{3}He. Unfortunately, there is no reasonable estimate of how many of these liquid channels there might be. In the pressure range we have studied, the diameter of these channels can be calculated [30] to be 6–31 nm; the higher the pressure, the smaller the channel diameter. In the most extreme example, if one such liquid channel were to span the distance between the Vycor rods with diameter of 20 nm, to fill it with ^{3}He would require 1.4×10^{11} atoms. To take a specific case, if we take a 10 ppm ^{3}He concentration for the ^{3}He in the solid, there are enough ^{3}He atoms present in our solid mixture sample to fill $\sim 3 \times 10^6$ such channels. Although we do not have a good estimate of the number of such channels, given the expected diffusion times, it appears that diffusion to such channels would be a fast process. Thus, the presence of ^{3}He would be expected to block flow through them.

In the work reported in Ref. [31], torsional oscillator (TO) measurements to determine the superfluid density, ρ_s, were carried out for nanometer-size channels (folded sheet mesoporous materials) of diameter $D = 1.5$–4.7 nm [31,32] filled with superfluid helium. This study revealed a transition from a Kosterlitz-Thouless behavior to a 1D-like temperature dependence of the apparent superfluid density only for $D <$ 2.2 nm. The temperature dependence they found, ρ_s for $D = 1.8$ nm [31], can be well fit by Eq. (5), which has been chosen to fit our flux temperature dependence, $F(T)$ (see Fig. 19). A value of $E \sim 0.4$ K for the parameter E is found for the data of Ref. [31]. This functional dependence, which is not present in the work of Ref. [31] above $D = 2$ nm, lends support to the notion of a 1D scenario for our observed flux and at least suggests that the liquid channels that are predicted would be too large in diameter to demonstrate 1D behavior.

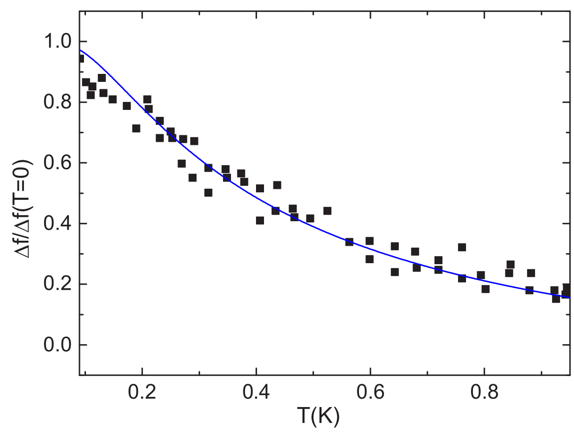

FIG. 19. (Color online) Temperature dependence of the torsional oscillator data from Ref. [31] for a pore diameter of 1.8 nm. Here, $\Delta f/\Delta f(T=0)$ is the relative frequency shift seen in the torsional oscillator as a function of temperature. The smooth curve is a fit of the data directly to Eq. (5) that we have used to characterize the universal temperature dependence of our flux through solid helium; we find, in this case, $E \sim 0.4$ K. If we convert to a flux resistance in this case, the power law, given by Eq. (6), does not provide a reasonable fit.

2. *Wall effects*

Instead of liquid channels that might form at grain boundaries, one might consider the possibility that a rough cell-wall surface might create a percolating liquid pathway along the cell wall that might carry a flux. We doubt that this is a possibility because if this were the case, it is unlikely that warming the solid and then cooling it would remove the ability of such percolating liquid to show mass flux. These rough-valley wall pathways should persist on thermal cycling. But, a thermal cycle above 650 mK typically causes a substantial reduction in the measured flux on subsequent cooling. This same reasoning concerning the behavior in response to thermal cycles should also apply to the possibility of liquid channels at grain boundaries unless annealing destroyed them.

Recently, Livne *et al.* [33] have reported measurements of the macroscopic relative motion of grains of solid ^{4}He. What relation that evolving work may have to mass flow studies is not yet clear.

3. *Dislocations*

Based on the possibility of 1D conducting pathways [34], one approach is to assume that ^{3}He impurities bind on dislocation cores (or their intersections) in the solid helium and block the flux that is carried by such pathways. This notion is supported by QMC simulations [35] that show that ^{3}He impurities diminish the superfluid density along the core of screw dislocations in hcp ^{4}He by binding on them. To illustrate this point, the inset to Fig. 13 shows $\ln(\chi)$ vs $1/T$. Straight lines here are presented by $\chi = \exp(-R/T)$, with R approximately independent of temperature, and $R = 0.94$ and 1.02 K for solid-solid (dashed curve) and solid-liquid (solid curve) bulk phase separation, respectively [13]. A fit of the T_d data (squares, dark solid line) by $\chi = \exp(-R/T)$ gives $R = 1.11$ K. A model [13] that includes a small number of binding sites for ^{3}He or ^{4}He atoms yields the function form $\chi = \exp(a - R/T)$, where $\exp(a)/[1 + \exp(a)]$ is the minimum impurity concentration that blocks superflux, and R includes the binding energy. This function form gives better fit (solid red line), with $R = 1.32$ K and $a = 2.18$. The numbers reported in this paragraph are revisions of those previously reported [13] because they take into account the temperature scale revision mentioned earlier in this report. This energy value is higher than the measured [36–38] and predicted [35,39] binding energy ($\sim$0.7 K) of single ^{3}He atoms to dislocations. Although to our knowledge it has not been calculated, the binding energy to dislocation intersections should exceed this. These facts are not inconsistent with the possibility that the flux extinction results from the ^{3}He binding to dislocation intersections [35], where the ^{3}He blocks the flux. To our knowledge, the binding energy for ^{3}He at the intersections of dislocations has not been considered theoretically and is not known.

It is perhaps useful to carry out qualitative numerical estimates that relate to the decoration of such cores (or intersections) with ^{3}He atoms. We will do this in this section and again later with the recognition that at times the choices we make will be arbitrary. There are a number of unknowns. One of these is the number of such structures that span the cell, Vycor to Vycor. We previously took [12] this number to be of the order of 10^5. If we take the solid ^{4}He density to be $\approx 2.9 \times 10^{22}$ atoms/cm^3, we find that about 6×10^7 ^{4}He atoms would be along a 2 cm direct strictly 1D pathway between the two Vycor rods; a pathway of diameter $\sim$1 nm [34] would require $\sim 5 \times 10^8$ atoms. Thus, to fully decorate 10^5 such cores would require $\sim 10^{13}$ atoms (or $\sim 10^{14}$ for a 1-nm-diameter case). Since Corboz *et al.* [35] have shown that the decoration of dislocation cores does not have to be complete to influence the superfluidity on the core, we rather arbitrarily take a smaller number, $\sim 1 \times 10^{12}$ atoms. Of course, a much smaller number could also be relevant since only a local dense decoration would be needed along a short segment of a dislocation core or at an intersection to substantially reduce the flux. Nonetheless, we continue with this number. Now, in our experimental geometry, a ^{3}He concentration of 10 ppm results in the presence of about 5.4×10^{17} ^{3}He atoms in the cell, which, if uniformly distributed, is a ^{3}He density of 2.9×10^{17} atoms/cm^3.

So, we can ask from what volume the needed number of atoms (e.g., for the 10^{13} case) would have to diffuse in the solid to decorate the dislocation cores. If we assume that these atoms diffuse from a cylindrical region to a dislocation core on the axis of the cylinder, we can estimate the radial distance from the core over which they would have to travel. We find this radial distance to be $\sim 1.5 \times 10^{-4}$ cm. We can then ask how long this will take. Those from a region near the core will arrive relatively quickly, while those from further away (an increasing number in any radial interval) will arrive later. For this, we take the ^{3}He diffusion constant near 26 bar and 100 mK at $\sim$10 ppm (extrapolating from the work of Eselson *et al.* [40]) to be $D \approx 1.5 \times 10^{-6}$ cm^2/sec and $\langle x^2 \rangle \sim 6Dt$, where t is the time, and we find the time to be about 2.5×10^{-3} seconds. For higher ^{3}He concentrations, the atoms would have to travel less far, but for higher concentrations, the diffusion constant is smaller. The time for flux recovery at T_d is well documented in Fig. 6, but the time for flux extinction is not yet well determined; we can only say that it is apparently less than $\sim$200 seconds. In spite of the approximations involved, if we compare the computed numbers for diffusion times with the times cited near Figs. 5 and 6 for the flux to be extinguished or recover, we conclude that diffusion of ^{3}He from the solid to dislocations or their intersections is not likely the controlling constraint in the flux change at T_d. The diffusion would likely be a rather fast process for the concentrations that we have studied.

4. A helium film

Another unlikely possibility is the flow of a helium film along the surfaces of the Vycor and the experimental cell. Were this to be the cause of the mass flux, one might expect that the temperature dependence would behave like a Kosterlitz-Thouless transition. This behavior is not evident in the data shown in Fig. 4 or other similar sets of data. Nonetheless, we might imagine a surface layer of liquid ^{4}He at the walls with a thickness of two atomic layers. Such a liquid ^{4}He layer is known to be located adjacent to a semisolid layer next to a wall in liquid mixture situations. The number of ^{4}He atoms involved would be $\sim 1.4 \times 10^{16}$. At 1 ppm ^{3}He, this is approximately the number of ^{3}He atoms in the cell. Given diffusion times, it is conceivable that such a film could be poisoned. But, the fact that annealing reduces or eliminates the ability of the solid to carry a flux when subsequently cooled argues strongly against a superfluid film as the carrier of the flux.

5. Vycor pore openings

Another possibility for what causes a reduction in the flux at T_d is ^{3}He accumulation at the openings to the Vycor pores. This possibility has recently been emphasized by Cheng *et al.* [41]. In their experiments, a variation of our approach was used. Instead of a superfluid-solid-superfluid geometry, they used a solid-superfluid-solid geometry. They were able to observe some temperature dependencies that are similar to those we have found in our various experiments, particularly the presence of T_d. In their discussion of the pore opening scenario, which they supported by calculations of the temperature-dependent binding of ^{3}He to various possible binding sites, the picture is that at T_d the ^{3}He moves to the solid-liquid interfaces at the openings of the Vycor pores. Cheng *et al.* [41] suggest that the ^{3}He atoms decorate the solid surface at the pore openings. Another possibility could be accumulation of ^{3}He at the pore ends.

For the flux to be fully blocked by ^{3}He in this scenario, the openings of the pores where the superfluid in the Vycor meets the solid must be blocked by ^{3}He. For our experimental apparatus, each Vycor rod surface meets the solid ^{4}He over a macroscopic surface area of about 0.3 cm^2. Given the properties of Vycor, we estimate that the open area of this surface that is comprised of pore openings is no less than 0.084 cm^2. Each pore of diameter 7 nm will have an open area at the surface of the Vycor no less than 3.84×10^{-13} cm^2. The number of such pore openings is estimated to be at least

2.18×10^{11}. All of these need to be blocked by ^{3}He. How much is needed at each pore opening? It is not clear that one monolayer would be adequate. If accumulation in the pore opening is responsible, more would be needed. So, as a specific case, we take as an estimate a distance along the pore of two pore diameters and presume that if this volume were to fill with ^{3}He, the pore would be blocked. This choice is certainly arbitrary; a greater or smaller length certainly might be appropriate. But, this choice might be appropriate for a model in which the ^{3}He blocks the pore itself by filling it at the end. In the vicinity of 100 mK, the expected phase separation for a liquid ^{3}He-^{4}He mixture indicates that if the ^{3}He were to be in the pores and blocking the flux, it would be due to a high-concentration normal mixture in the pores. Clearly, our numbers provide only a rough estimate, but it is not unreasonable. As we will show, there is more than enough ^{3}He for the pore-blocking scenario.

To fill such a volume for all of the pores would require $\approx 2.6 \times 10^{15}$ atoms. At 10 ppm, this is about 0.5 percent of all of the ^{3}He available; for higher (lower) concentrations, it is a proportionally smaller (larger) fraction. So, we can ask in this case about how long it will take for the ^{3}He to accumulate at the pore openings by migration from the solid. We take the same parameters of 26 bar, 10 ppm ^{3}He with a diffusion constant of $\approx 1.5 \times 10^{-6}$ cm^2/sec and note that the ^{3}He will have to travel macroscopic distances. For the case of 10 ppm ^{3}He, we find that the time required is $\sim$20 seconds. It is much shorter if all that is required is the appearance of a monolayer on the solid surface. Changing the concentration changes the time required; increasing the length of the pore that needs to be filled with ^{3}He increases it. These estimates are short times compared with the times shown for recovery of the flux documented in Fig. 6, especially when it is recognized that as ^{3}He accumulates in the solid near a pore opening, the local concentration may increase, which will cause the diffusion constant to decrease [40]. Were the ^{3}He to accumulate at the solid-liquid interface from a liquid mixture in a pore, we estimate that the time would be fast ($\sim$msec). As we have noted, flux extinction is complete in $\sim$200 seconds; recovery is complete in $\sim$500 seconds. These equilibration times are substantially longer than the diffusion estimates, unless, for example, the diffusion is from the solid and a much longer pathway in a pore must accumulate ^{3}He for the flux to be blocked. One fact that lends support for the mixture solid as the source of the ^{3}He is the fact that the T_d vs χ behavior closely resembles the phase-separation locus (solid line in Fig. 13). There is a need for more work to better understand the duration time for flux recovery and the details of how the ^{3}He manages to cause the conductance transition.

To explore the flux increase for $T < T_d$ at the lowest concentrations, it may be that the ^{3}He is exhausted and incompletely effective in blocking the flux from the pores. For the case of 0.17 ppm ^{3}He, the filled cell will have 9.2×10^{15} ^{3}He atoms in it. As we have noted, to fill the pores to a depth of two pore diameters will require $\approx 2.6 \times 10^{15}$ atoms. We have seen that the flux recovers for ^{3}He concentrations up to 10 ppm (in which case there are 5.4×10^{17} ^{3}He atoms in the cell). These estimates have a number of assumptions; in spite of them, it is not clear why there is not enough ^{3}He to completely block the flux. The transition to low flux for low concentrations is not complete. One possible cause for this, if the ^{3}He source is the solid, is that at a given temperature, which is T_d for the concentration in the solid, once ^{3}He atoms begin to leave the solid matrix, the solid now contains a lower concentration of ^{3}He. This naturally shifts the T_d to a lower temperature and at the given temperature no additional ^{3}He atoms leave the matrix. This observation explains the fact, clearly seen in, for example, Fig. 4 and evident in other data sets, that the flux in the middle of the T_d region is stable if the temperature is fixed [17]. That is, the data taken while cooling or warming is stable once a fixed temperature is achieved.

6. Behavior above and below T_d

It is not clear what might explain the universal temperature dependence above T_d. And, unless the estimates made here are substantially in error, it is also not fully clear why the flux increases for low ^{3}He concentrations below T_d. One possibility below T_d is that if the ^{3}He has been exhausted, but the blockage incomplete, then a lower temperature could be expected to provide an increase in the superfluid density in the confining conductance pathway.

In very recent work we have reported evidence that for the region of universal temperature dependence, $T > T_d$, the limitation to the flux is unrelated to the Vycor interface with the solid and takes place in the bulk solid [22]. This suggests that this temperature dependence may be due to a temperature-dependent superfluid density along the conducting pathways. Additional work is currently in progress and will be discussed more extensively in a future paper.

IV. CONCLUSIONS

We find the presence of ^{3}He as an impurity in hcp solid ^{4}He has a strong effect on the sharp flux reduction at a concentration-dependent characteristic temperature T_d. On the other hand, we find that the presence of ^{3}He does not alter the universal temperature dependence of the limiting mass flux above T_d. The magnitude of the flux is typically sample dependent, and sample dependent at any concentration, but the temperature dependence is universal. The specific reason for the universal temperature dependence for $T > T_d$ remains unresolved. It is likely due to the physics associated with the conducting pathways. The results also suggest that the presence of ^{3}He does not destroy the apparent Luttinger-like behavior of the flux. More experimental and theoretical study of solid helium and 1D superfluidity [7,31,42] and its pressure dependence are certainly needed.

ACKNOWLEDGMENTS

We appreciate the many conversations we have had with colleagues in the field, particularly B. V. Svistunov and W. J. Mullin. We also acknowledge the early work with the apparatus by M. W. Ray. This work was supported by the National Science Foundation Grant No. DMR 12-05217 and by Research Trust Funds administered by the University of Massachusetts, Amherst.

[1] V. L. Berezinskii, Sov. Phys. JETP **34**, 610 (1972).
[2] J. M. Kosterlitz and D. J. Thouless, J. Phys. C **6**, 1181 (1973).
[3] M. Boninsegni, A. B. Kuklov, L. Pollet, N. V. Prokof'ev, B. V. Svistunov, and M. Troyer, Phys. Rev. Lett. **99**, 035301 (2007).
[4] J. M. Luttinger, J. Math. Phys. **4**, 1154 (1963).
[5] A. Del Maestro and I. Affleck, Phys. Rev. B **82**, 060515(R) (2010).
[6] A. Del Maestro, M. Boninsegni, and I. Affleck, Phys. Rev. Lett. **106**, 105303 (2011).
[7] B. Kulchytskyy, G. Gervais, and A. Del Maestro, Phys. Rev. B **88**, 064512 (2013).
[8] A. Del Maestro, Int. J. Mod. Phys. B **26**, 1244002 (2012).
[9] B. Svistunov, http://online.itp.ucsb.edu/online/smatter-m06/svistunov/ (unpublished).
[10] M. W. Ray and R. B. Hallock, Phys. Rev. Lett. **100**, 235301 (2008).
[11] M. W. Ray and R. B. Hallock, Phys. Rev. B **79**, 224302 (2009).
[12] Y. Vekhov and R. B. Hallock, Phys. Rev. Lett. **109**, 045303 (2012).
[13] Y. Vekhov, W. J. Mullin, and R. B. Hallock, Phys. Rev. Lett. **113**, 035302 (2014).
[14] Y. Vekhov, W. J. Mullin, and R. B. Hallock, Phys. Rev. Lett. **115**, 019902(E) (2015).
[15] M. W. Ray and R. B. Hallock, Phys. Rev. B **82**, 012502 (2010).
[16] Y. Vekhov and R. B. Hallock, Phys. Rev. B **90**, 134511 (2014).
[17] Y. Vekhov and R. Hallock [J. Low Temp. Phys. (to be published)].
[18] W. J. Mullin (private communication).
[19] T. E. Huber and H. J. Maris, J. Low Temp. Phys. **48**, 463 (1982).
[20] M. W. Ray and R. B. Hallock, Phys. Rev. Lett. **105**, 145301 (2010).
[21] D. O. Edwards and S. Balibar, Phys. Rev. B **39**, 4083 (1989).
[22] Y. Vekhov and R. B. Hallock, Phys. Rev. B **91**, 180506(R) (2015).
[23] M. Tian, J. Wang, J. S. Kurtz, Y. Liu, M. H. W. Chan, T. S. Mayer, and T. E. Mallouk, Phys. Rev. B **71**, 104521 (2005).
[24] G. V. Pai, E. Shimshoni, and N. Andrei, Phys. Rev. B **77**, 104528 (2008).
[25] K. Arutyunov, D. Golubev, and A. Zaikin, Phys. Rep. **464**, 1 (2008).
[26] B. V. Svistunov and N. V. Prokof'ev (unpublished).
[27] A. N. Gan'shin, V. N. Grigor'ev, V. A. Maidanov, N. F. Omelaenko, A. A. Penzev, E. Y. Rudavskii, A. S. Rybalko, and Y. A. Tokar, Low Temp. Phys. **25**, 592 (1999).
[28] D. O. Edwards, A. S. McWilliams, and J. G. Daunt, Phys. Rev. Lett. **9**, 195 (1962).
[29] T. N. Antsygina, V. N. Grigor'ev, V. A. Maidanov, A. A. Penzev, S. P. Rubets, E. Y. Rudavskii, A. S. Rybalko, E. V. Syrnikov, and K. A. Chishko, Low Temp. Phys. **31**, 1059 (2005).
[30] S. Sasaki, F. Caupin, and S. Balibar, J. Low Temp. Phys. **153**, 43 (2008).
[31] H. Ikegami, Y. Yamato, T. Okuno, J. Taniguchi, N. Wada, S. Inagaki, and Y. Fukushima, Phys. Rev. B **76**, 144503 (2007).
[32] J. Taniguchi, Y. Aoki, and M. Suzuki, Phys. Rev. B **82**, 104509 (2010).
[33] E. Livne, A. Eyal, Scaly, and E. Polturak, J. Low Temp. Phys. **180**, 185 (2015).
[34] Ş G. Söyler, A. B. Kuklov, L. Pollet, N. V. Prokof'ev, and B. V. Svistunov, Phys. Rev. Lett. **103**, 175301 (2009).
[35] P. Corboz, L. Pollet, N. V. Prokof'ev, and M. Troyer, Phys. Rev. Lett. **101**, 155302 (2008).
[36] M. A. Paalanen, D. J. Bishop, and H. W. Dail, Phys. Rev. Lett. **46**, 664 (1981).
[37] O. Syshchenko, J. Day, and J. Beamish, Phys. Rev. Lett. **104**, 195301 (2010).
[38] F. Souris, A. D. Fefferman, H. J. Maris, V. Dauvois, P. Jean-Baptiste, J. R. Beamish, and S. Balibar, Phys. Rev. B **90**, 180103 (2014).
[39] S. S. Kim, C. Huan, L. Yin, J. Xia, D. Candela, and N. S. Sullivan, Phys. Rev. Lett. **106**, 185303 (2011).
[40] B. Esel'son, V. Mikheev, V. Grigor'ev, and N. Mikhin, Sov. Phys. JETP **47**, 1200 (1978).
[41] Z. G. Cheng, J. Beamish, A. D. Fefferman, F. Souris, S. Balibar, and V. Dauvois, Phys. Rev. Lett. **114**, 165301 (2015).
[42] R. Toda, M. Hieda, T. Matsushita, N. Wada, J. Taniguchi, H. Ikegami, S. Inagaki, and Y. Fukushima, Phys. Rev. Lett. **99**, 255301 (2007).